Strategies to reduce the resistance sources on Electrochemical Double Layer Capacitor electrodes

Sonia Dsoke*, Xu Tian, Corina Täubert, Steffen Schlüter [1], Margret Wohlfahrt-Mehrens

Zentrum für Sonnenenergie- und Wasserstoff-Forschung Baden-Württemberg, Lise-Meitnerstraße 24, D-89081 Ulm, Germany

HIGHLIGHTS

- Electrode lamination has been optimized by adjusting pressure and temperature.
- Low contact resistance has been obtained by applying 50 bar and 160 °C.
- Conditions for preserving the electrode porosity are 10 bar and 200 °C.

ARTICLE INFO

ABSTRACT

Electrochemical double layer capacitors (EDLCs) are conceived as high power devices. Generally, power improvement is mainly related to lowering the device impedance ($P_{max} = V^2/4R$). However, the supercapacitor impedance is the sum of several contributions (electrolyte, active material, contact between the active material and the current collector, electrode porosity). In this work we demonstrate that the resistance at the interface between the electrode and the current collector and as well the diffusion resistance can be properly controlled during the electrode preparation. In our preparation method the electrodes are compacted by using a hot-press device. During the electrode fabrication parameters such as temperature and pressure are systematically modulated in order to find the best condition for increasing the contact between the electrode and the current collector while maintaining good electrode porosity.

© 2013 Elsevier B.V. All rights reserved.

1. Introduction

The number of applications requiring mobile power sources has increased dramatically in the past two decades. The energy storage research community has responded by producing batteries of excellent energy density and capacitors of remarkable power density. In this context, EDLCs are energy storage devices which are used in a wide range of consumer and industrial applications, such as advanced consumer electronics, implantable medical devices, electric vehicles, and high performance aircrafts [1]. EDLCs attracted considerable attention since they fill the gap between batteries and conventional capacitors in terms of energy and power density. However, improvements are required in order to make this technology competitive in applications where batteries or dielectric capacitors are currently used [2,3]. The energy of a supercapacitor is dependent on the capacitance and on the cell voltage by the relation $E = \frac{1}{2}CV^2$. Enhancement in capacitance can be obtained by optimizing carbon features such as pore size distribution and surface area [4,5]. On the other hand, the cell voltage can be increased by using asymmetric combinations of different cathode and anode materials [6–8]. Power improvement is mainly gained by lowering the device resistance ($P_{max} = V^2/4R$). However, the resistance of a supercapacitor is the sum of various contributions such as the electrolyte resistance, the particle–particle resistance, the contact resistance between the active material and the current collector and the resistance of the electrolyte within the porous structure of the active material [9,10]. Schematically, the resistance sources of a supercapacitor can be depicted as in Fig. 1. The intrinsic resistance of the electrolyte ($R_{electrolyte}$) and the diffusion resistance of the electrolyte into the porous structure of the activated carbon (R_{diff}) depend essentially on the specific features of the material used (electrolyte and activated carbon). On the other hand the boundary resistances at the interfaces carbon–carbon and carbon–current collector can be controlled during the electrode preparation. Every of these interfaces is associated to a boundary resistance and to

* Corresponding author. Tel.: +49 731 9530 560; fax: +49 731 9530 599.
E-mail address: sonia.dsoke@zsw-bw.de (S. Dsoke).
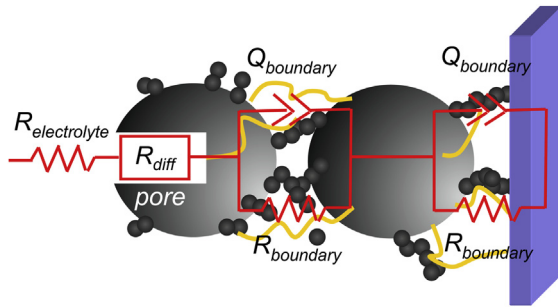[1] Present address: TUM CREATE 1 CREATE Way, #10-02 CREATE Tower, Singapore 138602, Singapore.

Fig. 1. Resistance sources in an EDLC electrode.

the related constant phase element which are in parallel ($R_{boundary}$ and $Q_{boundary}$ in Fig. 1). Another factor which has to be taken into account is the micro-sized porosity created by the particle packing. The interparticle pores (or voids) serve as electrolyte pathway and therefore they have a certain impact on the overall electrode kinetics [11].

This work is focused on the optimization of the electrode preparation with the aim of minimizing all resistance sources and preserving the optimal electrode porosity. Improvements have been obtained by laminating the composite carbon electrode on the Al current collector by using different pressures and temperatures. Furthermore, image analysis has been used in order to evaluate the textural properties of the electrodes and to estimate the macro-porosity and compaction level for each hot-pressing condition.

2. Experimental

2.1. Electrode preparation

The electrodes used in this study have been prepared by employing commercially available materials (i.e., porous carbon, binder, conductive carbon, current collector, additives). Activated Carbon (AC) YP-17D from Kuraray Chemical Co. has been chosen as active material. The composite carbon electrodes have been prepared by mixing 85 wt % of the activated carbon with 5 wt% of carbon black (DENKA, Japan) as conductive agent and 10 wt% of polytetrafluroethylene (PTFE) as binder (3M Company). The components have been first mixed in a dry way using a ball milling, then compacted using a mortar and finally calendered in order to obtain a free-standing film with a final thickness of about 90–120 μm. An etched aluminum foil (from JCC, Japan) has been employed as current collector and pre-treated with a commercial conductive paint (Electrodag® EB-012 by Acheson Colloids Company) before use.

Free-standing electrodes of 25 cm² area have been then pressed on the current collector for three minutes using different pressures and temperatures.

Two different experiments have been performed in order to distinguish between the effects of pressure and temperature. In the first experiment the temperature was kept constant at 160 °C and the pressure was varied from 10 to 50 bar. In the second experiment the pressure was maintained at the constant value of 10 bar and the temperature was increased from 160 °C up to 250 °C.

The influence of the current collector type on the adhesion has been as well investigated. Two different current collectors have been chosen: an aluminum grid and an etched aluminum foil. Both were pre-treated with Electrodag® EB-012.

2.2. Capacitor assembly

The capacitor consisted of two identical electrodes separated by three glass microfiber filter separators (GFA) and assembled in a Swagelok® type cell with stainless steel current collectors. 1 M tertraethylammonium tetrafluoroborate (TEABF₄) in acetonitrile (Honeywell) has been used as electrolyte. Before cell assembly in an Ar-filled glove box (MBraun), the electrodes have been dried at 130 °C under vacuum overnight in order to remove traces of water.

2.3. Electrochemical characterization

All the measurements have been performed at room temperature with a VMP3 multi-channel potentiostat/galvanostat (Bio-logic Science Instrument), equipped with an EC-Lab® software.

Cyclic Voltammetric (CV) curves have been recorded at 10 mV s⁻¹ in the potential range 0 V–2.5 V. Galvanostatic Cycling with Potential Limitation (GCPL) has been carried out at 1 A g⁻¹ in the same potential range. Electrochemical Impedance Spectroscopy (EIS) measurements have been performed by applying a low amplitude alternating voltage of 5 mV at a bias voltage of 0 V (fully discharged state) and the frequency has been ranged from 100 kHz to 10 mHz. The EIS spectra have been analyzed using the non least-square fitting program EQUIVCRT developed by Boukamp [12].

2.4. Textural−morphological characterization

SEM pictures have been collected on Au-sputtered electrodes. The sputtering treatment has been used in order to detect all the electrode components including the binder. SEM measurements have been made using a LEO 1530-VP-Gemini microscope from Zeiss. In order to evaluate the macro-porosity and particle packing of the electrodes the images have been analyzed using ImageJ, a public domain, Java-based image processing software.

3. Analysis methodologies

3.1. Determination of specific capacitance

The cell capacitance, using a galvanostatic method, is normally deduced from the slope of the discharge curve (Fig. 2) by using the equation below:

$$C = i/(dV/dt) \tag{1}$$

where C is the cell capacitance in Farad (F), i the discharge current in Ampere (A) and dV/dt is the slope of the discharge curve in Volt per second (V s⁻¹).
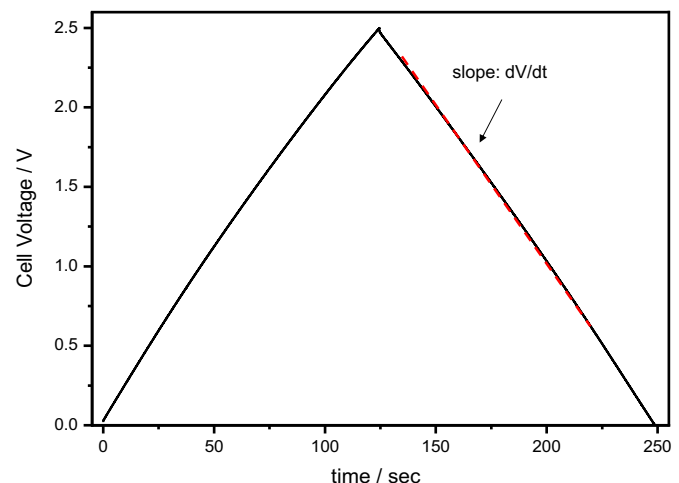

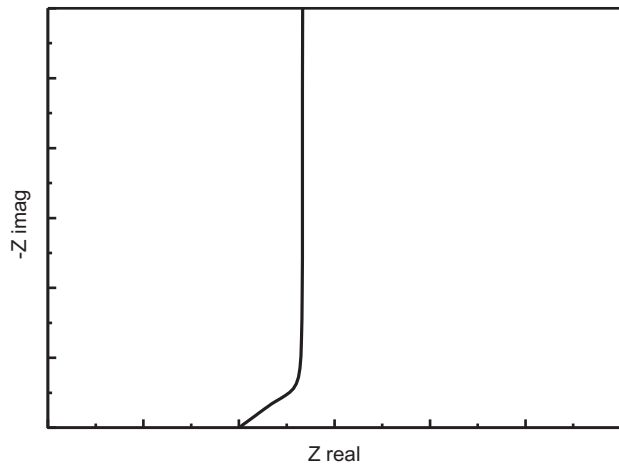**Fig. 2.** Charge−discharge curve of a supercapacitor cell.

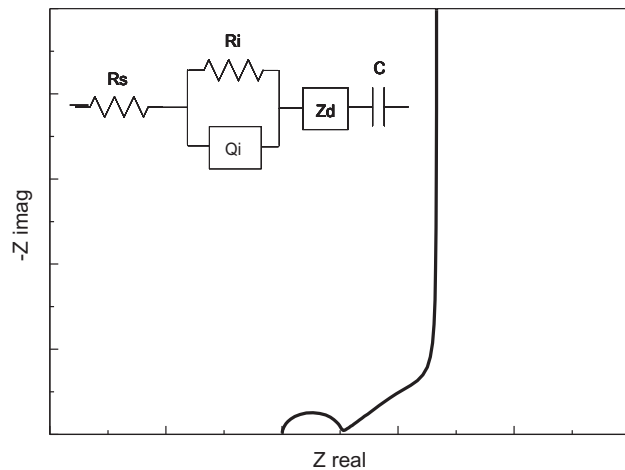**Fig. 3.** Typical Nyquist plot for a carbon/carbon supercapacitor.

Fig. 4. Experimental Nyquist plot and corresponding simulation. The inset shows the equivalent circuit used for the simulation.

The following equation applies for a two-electrode system, assuming that the electrodes have the same weight:

$$C_{cathode} = C_{anode} = C \qquad (2)$$

In this case, the measured cell capacitance is:

$$C_{cell} = C/2 \qquad (3)$$

The specific capacitance (C_{spec}) in Farad per gram of active material (F g^{-1}) is related to the capacitance of the cell (C_{cell}) by:

$$C_{spec} = 2C_{cell}/m_{AM} \qquad (4)$$

where m_{AM} represents the active material weight of each electrode.

3.2. Electrochemical Impedance Spectroscopy

A typical Nyquist plot for an EDLC based on porous carbon shows from high to medium frequencies a typical diffusion region which reflects the resistance of the electrolyte through the electrode pores. The diffusion part is then followed by a vertical line, indicating a capacitive behavior (Fig. 3).

However, experimentally, a Nyquist plot of a carbon electrode shows a semicircle at high frequencies which shifts the total resistance towards higher values as depicted in Fig. 4. This semicircle is quite common and is reported by several other groups as well [13–15].

There are various hypotheses that might explain the nature of this semicircle. In the case of activated carbons with functional groups operating in an aqueous electrolyte it can be correlated to the charge transfer corresponding to faradaic processes [15]. Moreover, it can be associated to the poor electronic conductivity among the particles (activated carbon–activated carbon and activated carbon–carbon black contacts). Furthermore, another possible explanation can be the poor contact between the current collector and the composite electrode [13]. In general, the poor contact at the interface between electrode and current collector is a critical and persistent problem not only on the supercapacitor development but also on the Li-ion battery manufacturing. Recently, M. Gaberscek et al. [16] investigated the influence of different current collectors on the kinetics of Li-ion battery electrodes. Gaberscek et al. found a direct correlation between the semicircle at high frequencies detected in the Nyquist plot and the interface between the current collector and the composite electrode.

With this work we confirm that also in the case of carbon/carbon supercapacitors this semicircle can be associated to the poor contact between the current collector and the composite electrode.

The equivalent circuit used for simulating the impedance spectra is shown in the inset of Fig. 4. The circuit may be rewritten, using the Boukamp's notation [12], as $LR_{el}(R_iQ_i)TQ_{dl}$ where L represents the inductive contribution of the cables, R_{el} is the electrolyte resistance, (R_iQ_i) represents the resistance and the constant phase element associated to the semicircle, T is the finite-diffusion element and Q_{dl} is the constant phase element associated to the double layer capacitance. The commonly used equation for simulating the diffusion impedance of electrochemical double layer supercapacitors [17,18] is:

$$Z_W(\omega) = Z_0(J\omega)^{-1/2}\coth\left[B(J\omega)^{-1/2}\right] \qquad (5)$$

where Z_0 and B are the Warburg factors [18]. The results of the non-linear regression analysis showed that the Nyquist plots can be
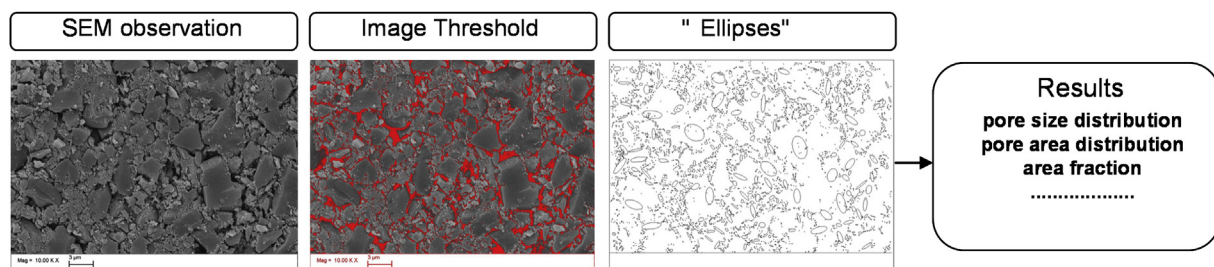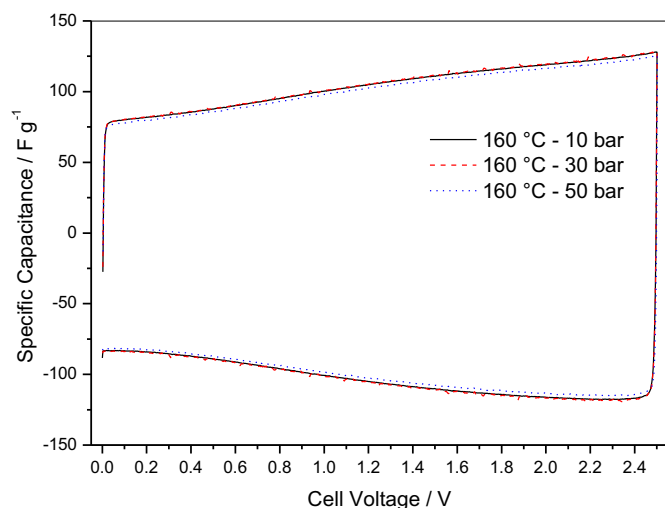

Fig. 5. Image processing steps for the pores characterization.

Fig. 6. Specific capacitance versus cell voltage of carbon electrodes prepared at various pressures. The data are obtained from CV at 10 mV s^{-1} by dividing the specific current by the scan rate. Electrolyte: TEABF$_4$ in Acetonitrile.

Fig. 8. Nyquist plots of cells assembled with electrodes pressed on a treated Al foil at 160 °C and at 10, 30, and 50 bar. Electrolyte: TEABF$_4$ in Acetonitrile. The inset shows the Nyquist plots magnification.

well simulated by using the equivalent circuit mentioned above (see simulated and measured curves in Fig. 4). The "chi-squared" parameter (χ^2, i.e. the sum of the square of the differences between measured and simulated points) which is an indication of the quality of the fit [12] has a value of about 10^{-5}. In general, a value of 10^{-5} or less for χ^2 indicates a reasonable to a good fit.

The simulation allowed us to extract the parameters of interest, which in this paper are essentially the resistance related to the semicircle and the resistance related to the diffusion.
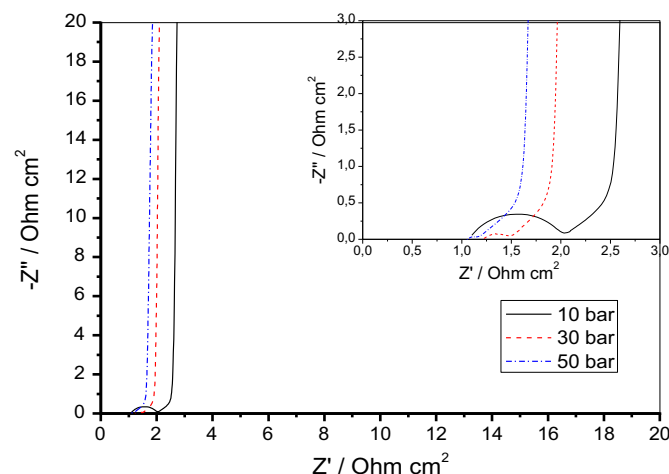
Since the thickness of the electrode (which in our case ranges from 90 to 120 μm) is directly proportional to the diffusion resistance, the "diffusion resistivity" has been calculated:

$$\rho_{\mathrm{d}} = (R_{\mathrm{d}} \times A)/L \qquad (6)$$

where ρ_{d} is the diffusion resistivity, R_{d} is the diffusion resistance as calculated from the impedance simulation, A represents the geometric area of the electrode and L the thickness of the electrode.

3.3. Image analysis methodology

Image processing of scanning electron micrographs is a very powerful tool on understanding the textural properties of composite materials. ImageJ is a public domain, Java-based image

processing program. It has been widely used to display, edit, process and analyze 8-bit, 16-bit, and 32-bit images [19,20]. In this work, ImageJ has been used to analyze the pore size of the composite carbon electrodes prepared at different hot-pressing conditions. The purpose was to observe the effect of temperature and pressure on the particle packing and morphology and thus to have a direct correlation with the electrochemical results.

The image processing steps are described in Fig. 5. The SEM pictures have been first converted to binary images by selecting an appropriate threshold value. Then the area of the pores has been calculated using the "Analyze Particle" function on the ImageJ program menu by fitting the pores with ellipses. The total number of the analyzed pores taken from two individual SEM images for each sample is sufficient for exhibiting the differences in the pore structure (2500–5000 counts for samples).

4. Results and discussion

4.1. Pressure effect

The first objective of this work was to investigate the effect of the pressure on the electrochemical performance of the carbon electrode. With this purpose, electrodes have been laminated onto the aluminum current collector by using the same temperature (160 °C) and applying 10, 30 and 50 bar, respectively. As shown in
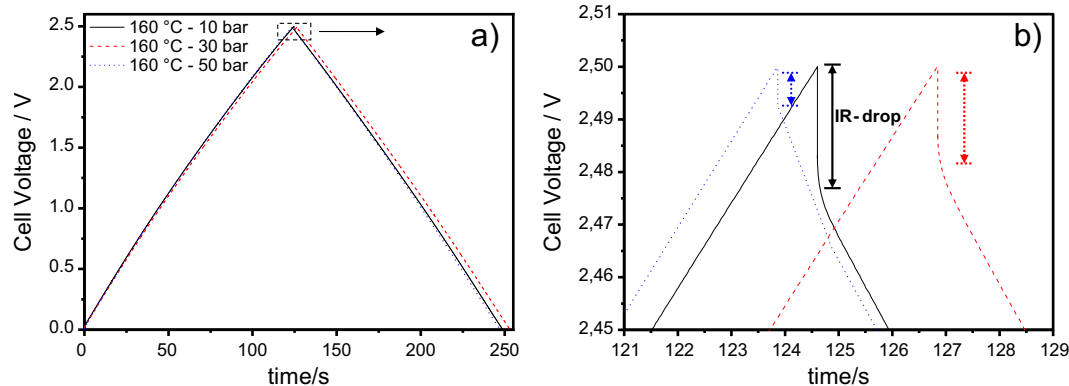
Fig. 7. (a) Galvanostatic cycle at 1 A g^{-1} of carbon electrodes pressed on a treated Al foil at 160 °C and at 10, 30, and 50 bar. (b) Magnification of the curves at more positive potentials. Electrolyte: TEABF$_4$ in Acetonitrile.
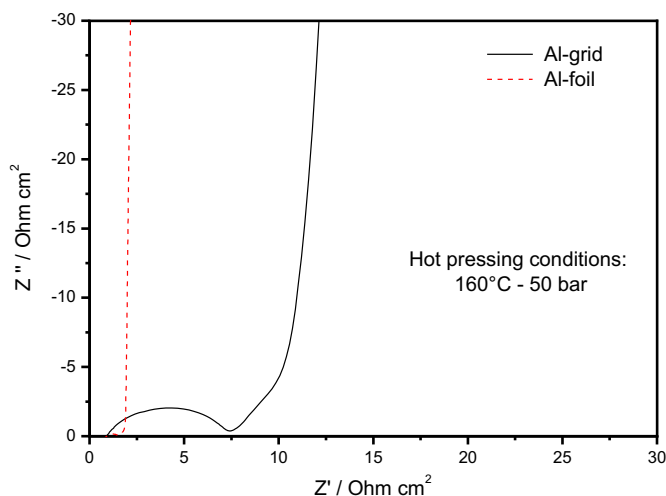
Fig. 9. Impedance spectra of electrodes pressed using the same conditions (160 °C and 50 bar) but onto different current collectors.

Fig. 11. Pores area calculated by using ImageJ analysis of the electrodes of Fig. 10.

Fig. 6 the voltammogram shape is retained for all the investigated electrodes. This suggests that no modifications occur on the micro-pores (i.e. pores smaller than 2 nm) of the activated carbon after the electrode compaction at different pressures.

Moreover, the capacitance values are confirmed by the galvanostatic cycles performed at 1 A g^{-1} (Fig. 7a). The electrodes deliver very similar capacitance values: 104, 104.7 and 102.6 F g^{-1} for electrodes pressed at 10, 30 and 50 bar, respectively. These results suggest that the micro-porous structure (which is directly related to the capacitance) of the activated carbon is not much influenced by the pressure applied on the electrodes. The magnification of the galvanostatic cycle at more positive potentials allows estimating the IR-drop of the cell. As depicted in Fig. 7b the ohmic drop is strongly dependent on the pressure used for preparing the electrodes: the lower the pressure the higher is the ohmic drop. However, the calculation of the IR-drop gives only an indication of the total resistance of the cell, but does not allow an understanding of the specific contributions of the various electrode components to
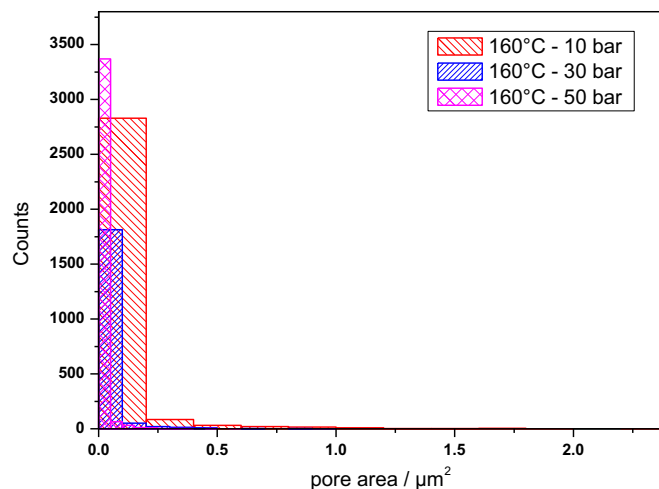
the overall cell resistance. A deeper understanding can be obtained by analyzing the EIS data. Fig. 8 shows the Nyquist plots of the electrodes treated at the various pressures. When the electrode is pressed at 10 bar a significant semicircle at high frequencies is present. By raising the pressure, the diameter of this semicircle decreases linearly. At 50 bar the semicircle almost disappears and the related Nyquist plot is close to the ideal behavior of a porous electrode. As it was already discussed in Section 3.2, the linear decrease of the semicircle with the pressure can be correlated either to an improvement of the contact at the interface aluminum/carbon electrode or to a better internal particle–particle contact. The latter can be achieved, if the electrode material is properly compacted. However, if two electrodes are compacted using the same conditions (50 bar and 160 °C) but attached onto different current collectors — i.e., Al grid or Al foil — the resulting Nyquist plots show significant differences in the semicircle diameter (Fig. 9). This means that the semicircle at high frequencies can be correlated to the interface electrode/current collector rather than to the particle–particle contact. The different lengths of the 45° slopes
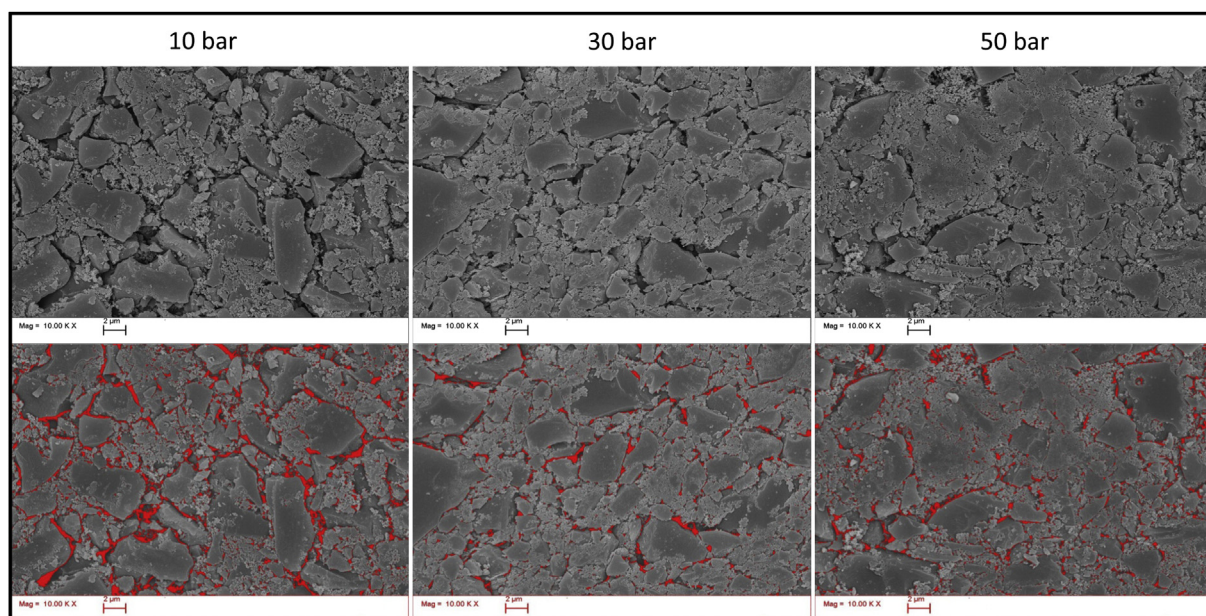

Fig. 10. Original and with ImageJ-converted micrographs of the electrodes pressed at 160 °C and different pressures.

in Fig. 9 are simply due to the differences in the electrode thickness and it is not correlated to the current collector type.

From the results of Fig. 8 it is clear that the best conditions for attaching the electrode to the current collector (in this case etched aluminum foil) are 50 bar and 160 °C. However, it is also important to consider the effect of the pressure on the electrode porosity and particle packing. As a first approach the electrode bulk densities have been calculated. The density is slightly increasing with the applied pressure. In fact, the calculated values are 0.697, 0.715 and 0.719 g cm^{-3} for the electrode pressed at 10, 30 and 50 bar, respectively. In order to investigate the electrode morphology and porosity the SEM images have been analyzed by using the ImageJ software. Fig. 10 shows the original and the corresponding converted images (after applying a threshold) of the three electrodes under investigation.

The resulting histogram (Fig. 11) shows that the macro-pore area significantly reduces with the pressure. The average pore area is 0.018 μm^2 and 0.01 μm^2 for the electrode pressed at 10 and 50 bar, respectively.

More information about the electrode morphology can be obtained from the images at higher magnification (Fig. 12). As it is evident, excessive pressure causes a change in the binder morphology. While at 10 bar the PTFE binder retains its original spherical shape, at 50 bar the binder particles are much more compacted as shown in the dashed areas.

Therefore, even if 50 bar are very effective on reducing the contact resistance between the electrode and the current collector (see the disappearing of the semicircle at high frequencies in the Nyquist plot of Fig. 8), applying such a high pressure can also have a negative effect on the binder packing density and on the electrode porosity. One solution is to treat the electrode at higher temperatures while maintaining the pressure as low as possible.

4.2. Temperature effect

The temperature plays also an important role on the electrode preparation. As it is shown in the Nyquist plot of Fig. 13, at 200 °C a pressure of 10 bar is already enough to reach a good electrode adhesion (disappearing of the semicircle). This means, when using higher temperatures it is not anymore necessary to subject the electrode to such high pressures. In this way the electrode macro-porosity can be easily retained. In fact, no relevant morphological differences can be observed among electrodes treated at different temperatures (Fig. 14). The electrode porosity as calculated from the image analysis is very similar for the three electrodes. The average pore area is 0.018, 0.015 and 0.015 μm^2 for the electrodes pressed at 10 bar and 160, 200 and 250 °C, respectively.

The data obtained from the image analysis have been compared with the diffusion parameters obtained from the EIS analysis. As already explained in Section 3.2 the diffusion resistivity instead of the diffusion resistance has been calculated in order to avoid the influence of the electrode thicknesses. Fig. 15 reports these results for all the electrodes investigated in this work. A very good correlation can be observed between the pore dimension, as calculated
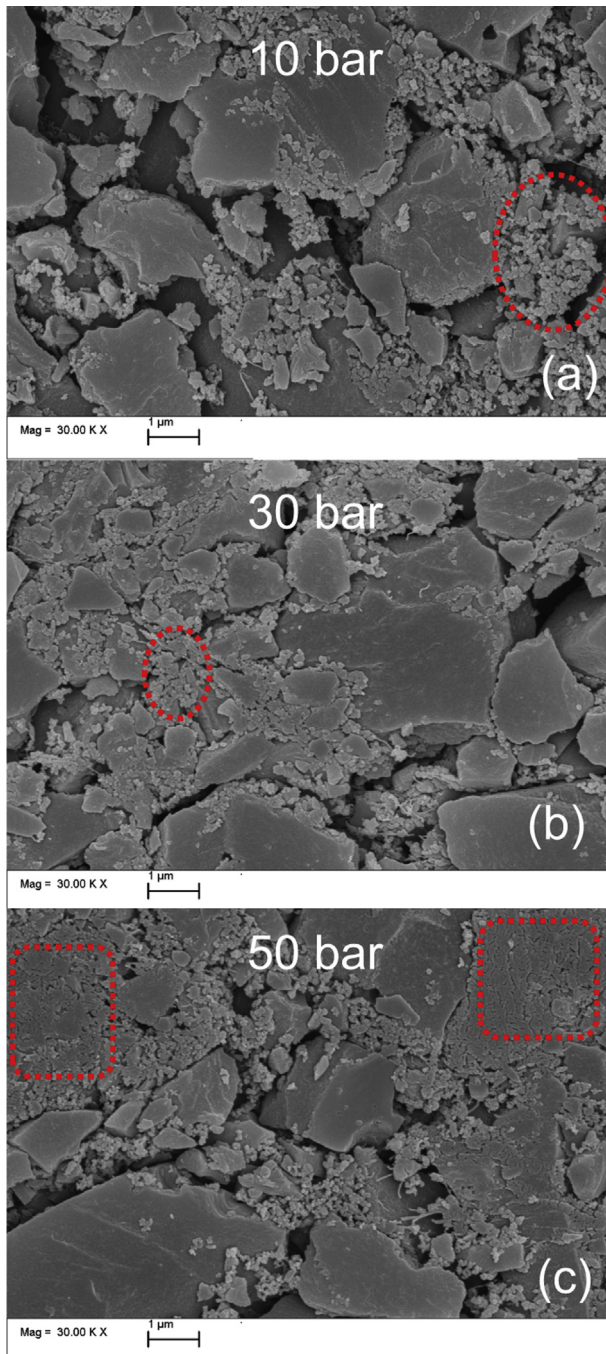
Fig. 12. SEM images at higher magnification of carbon electrodes pressed at 160 °C and at various pressures. The areas marked with dashed line indicate the binder.
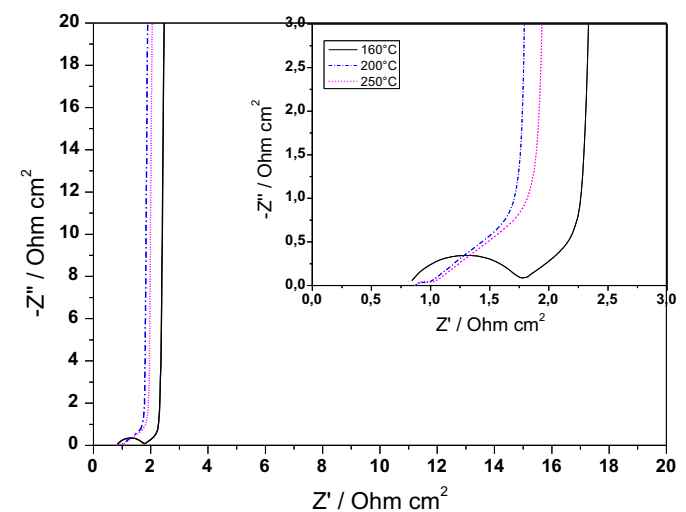
Fig. 13. Nyquist plots of cells assembled with electrodes pressed on a treated Al foil at 10 bar and at different temperatures. Electrolyte: TEABF$_4$ in Acetonitrile. The inset shows the Nyquist plots magnification.
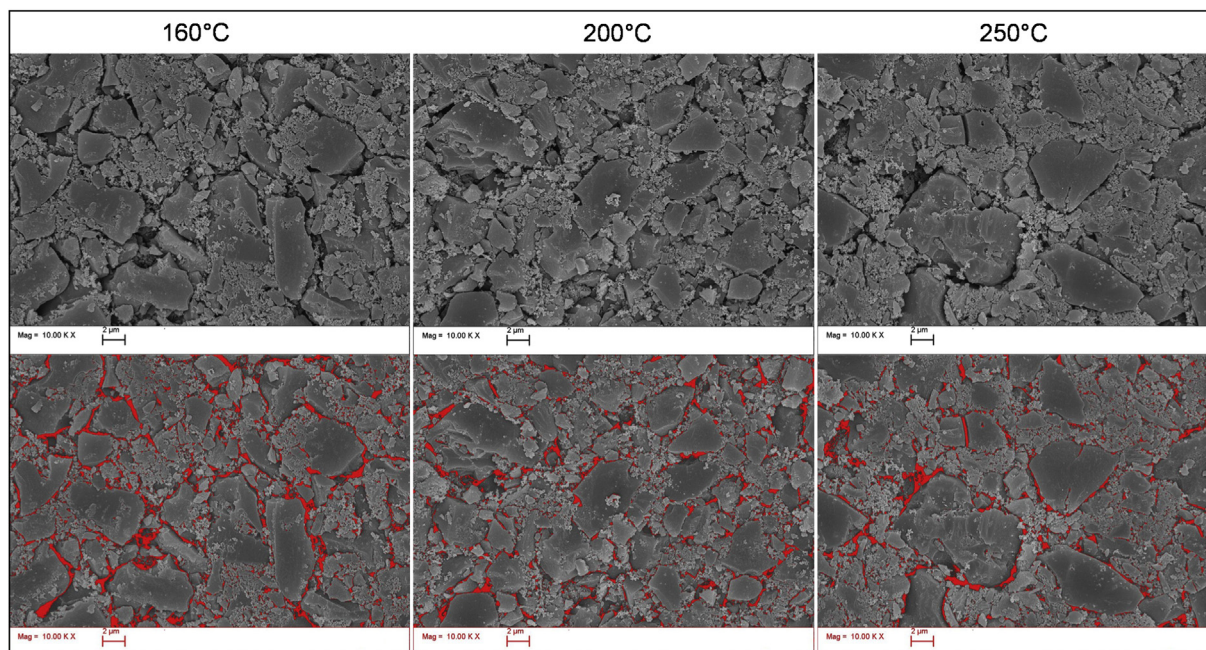
Fig. 14. Original and with ImageJ-converted micrographs after threshold of electrodes pressed at 10 bar and different temperatures.
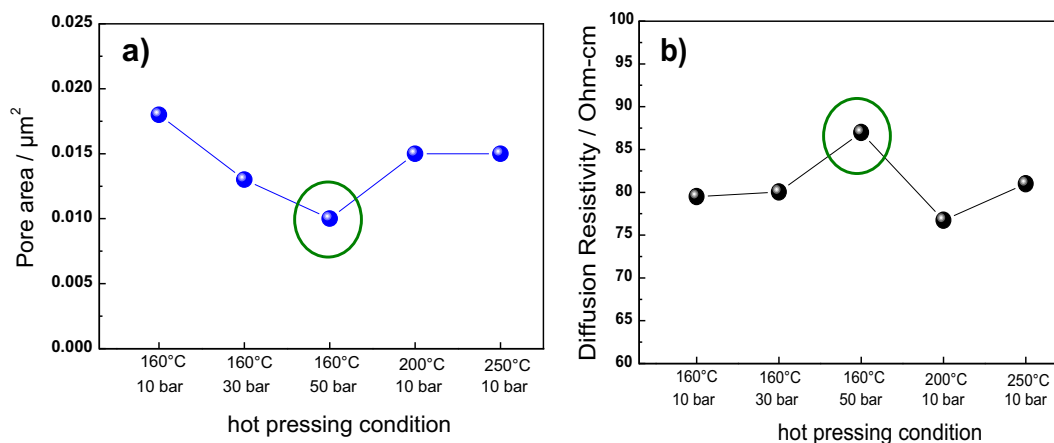

Fig. 15. (a) Pore area average calculated by SEM images using ImageJ software and (b) Diffusion resistivity as calculated from the EIS simulation.

from ImageJ analysis (Fig. 15a) and the diffusion resistivity of the electrolyte through the electrode pores as calculated from the fit of the EIS data (Fig. 15b). The two graphs are in a good agreement: the electrode pressed at 50 bar shows smaller macro-pores and higher diffusion resistivity. Therefore, the diffusion impedance (Z_d) is not only dependent on the micro-structure of the porous carbon used but is also influenced by the electrode macro-porosity and can be controlled during the electrode preparation. The macro-pores serve as electrolyte pathway and can influence the electrode kinetics.

5. Conclusion

With this work we demonstrated that some of the resistance sources can be adjusted during the electrode preparation. The choice of the hot-pressing condition is of fundamental importance for achieving low contact resistance and good electrode porosity.

The results of the impedance study showed that the contact resistance between current collector and composite electrode can be improved by properly regulating processing parameters,

i.e., temperature and pressure. Good adhesion has been reached by using a temperature of 160 °C and pressing the electrode at 50 bar. However, the SEM image analysis revealed that the electrode porosity and thus the electrolyte diffusion are reduced if the electrode is treated at such high pressure. This drawback can be easily solved by increasing the working temperature up to 200 °C and consequently decreasing the pressure to 10 bar. These conditions are sufficient for reaching a good electrode adhesion and at the same time maintaining good electrode porosity. This work can bring an important contribution to the EDLCs' electrode manufacturing in finding the proper conditions for the lamination of the electrode onto the current collector.

References

[1] A. Burke, J. Power Sources 91 (2000) 37–50.
[2] R. Kötz, M. Carlen, Electrochim. Acta 45 (2000) 2483–2498.
[3] M. Winter, R. Brodd, Chem. Rev. 104 (2004) 4245–4269.
[4] D. Qu, H. Shi, J. Power Sources 74 (1998) 99–107.
[5] M. Inagaki, H. Konno, O. Tainake, J. Power Sources 195 (2010) 7880–7903.
[6] I. Plitz, A. du Pasquier, F. Badway, J. Gural, N. Pereira, A. Gmitter, G.G. Amatucci, Appl. Phys. A 82 (2006) 615–626.
[7] D. Cericola, P. Novák, A. Wokaun, R. Kötz, J. Power Sources 196 (2011) 10305–10313.
[8] V. Khomenko, E. Raymundo-Piñero, F. Béguin, J. Power Sources 177 (2008) 643–651.
[9] P.L. Taberna, C. Portet, P. Simon, Appl. Phys. A 82 (2006) 639–646.
[10] C. Portet, P.L. Taberna, P. Simon, E. Flahaut, C. Laberty-Robert, Electrochim. Acta 50 (2005) 4174.
[11] A.G. Pandolfo, G.J. Wilson, T.D. Huynh, A.F. Hollenkamp, Fuel Cells 10 (2010) 856–864.
[12] B.A. Boukamp, Solid State Ionics 128 (1986) 31.
[13] C. Portet, P.L. Taberna, P. Simon, C. Laberty-Robert, Electrochim. Acta 49 (2004) 905.
[14] L. Xi-miao, Z. Rui, L. Dong-hui, Q. Wen-ming, Y. Jun-he, L. Li-cheng, New Carbon Mater. 22 (2) (2007) 153.
[15] D. Qu, J. Power Sources 109 (2002) 403.
[16] M. Gaberscek, J. Moskon, B. Erjavec, R. Dominiko, J. Jamnik, Electrochem. Solid State Lett. 11 (10) (2008) A170–A174.
[17] E. Lust, A. Jänes, T. Pärn, P. Nigu, J. Solid State Electrochem. 8 (2004) 224–237.
[18] L. Xi-miao, Z. Rui, Z. Liang, L. Dong-hui, Q. Wen-ming, Y. Jun-he, L. Li-cheng, New Carbon Mater. 22 (2007) 153–158.
[19] K. Ohzeki, K. Seino, T. Kumagai, B. Golman, K. Shinohara, Carbon 44 (2006) 578.
[20] M. Chang, J.R. Deka, C.T. Tszeng, P.R. Cheng, Desalination 234 (2008) 66.